Water SA 52(2) 111–122 / Apr 2026
https://doi.org/10.17159/wsa/2026.v52.i2.4231

Research paper

Hydrogeochemical processes and evolution of groundwater chemistry in a karst environment in Gauteng Province, South Africa

Lufuno Ligavha-Mbelengwa[1,2], Modreck Gomo[2], Dan J Lapworth[3] and Godfrey Madzivire[1]

[1]*Council for Geoscience, 280 Pretoria Street, Silverton 0184, Pretoria, South Africa*
[2]*Institute for Groundwater Studies, University of the Free State, PO Box 339, Bloemfontein 9300, South Africa*
[3]*British Geological Survey, Environmental Science Centre, Keyworth, Nottingham, NG12 5GG, United Kingdom*

Groundwater chemical composition is dependent on various natural and anthropogenic factors. This study assessed factors influencing the groundwater chemical composition in an environment controlled by geological structures. The study further examined the suitability of groundwater quality for domestic and irrigation use. A hydrochemical approach was used to evaluate the main processes and activities influencing the groundwater chemistry. The main hydrochemical facies identified were mixed facies dominated by Na^+ and HCO_3^- in the southwestern area, and MgCl / $MgClSO_4$ / $MgClHCO_3$, which dominated the northern area. Hydrogeochemical processes that were associated with the southwestern area groundwater were silicate weathering, ion exchange, carbonate and gypsum dissolution. The groundwater composition in the northern area, although controlled by carbonate dissolution, was influenced more by anthropogenic activities as indicated by the Cl/Br mass ratios of >88 and high Cl^- concentrations. The high Cl^- could not be attributed to halite dissolution due to its undersaturation in solution. Additionally, the northern area groundwater showed excess SO_4^{2-}, which was linked to anthropogenic contamination. Groundwater in the southwestern area was suitable for domestic use, while that in the northern area was classified as unacceptable. The multi-tool approach used in this study provided a clear contrast between the northern and southwestern areas' groundwater, showing that these were influenced by distinct factors. This underscores the importance of developing area-based protection and management strategies that consider both natural processes and anthropogenic impacts.

CORRESPONDENCE
Lufuno Ligavha-Mbelengwa

EMAIL
lligavhambelengwa@geoscience.org.za

DATES
Received: 24 July 2025
Accepted: 14 April 2026

KEYWORDS
anthropogenic activities
geological structures
groundwater quality
hydrochemical facies
saturation indices

INTRODUCTION

Groundwater composition is controlled by various natural factors, including hydrogeochemical processes, hydrological factors, and geological structures (Jalali, 2007). During rock–water interaction, hydrogeochemical processes result in the release of ions into groundwater through the weathering and dissolution of associated mineral phases (Pawar, 1993), evolving groundwater from one chemical composition to another. Apart from the natural processes, groundwater is also vulnerable to anthropogenic activities, which can largely influence its overall quality (Katz et al., 2009; Mokadem et al., 2021; Lukač Reberski et al., 2022). Karst aquifers are the most vulnerable because of fast flow rates, leading to low natural attenuation during recharge (Katz et al., 2009; Lukač Reberski et al., 2022). The karst aquifers of the Transvaal Supergroup are important groundwater resources in South Africa (Schrader and Winde, 2015), primarily used for domestic, irrigation and mining purposes (Abiye et al., 2011; DWA, 2013). Mokadem et al. (2021) and Abiye et al. (2011) reported contamination of karst aquifers in the Witwatersrand Goldfields by local anthropogenic activities such as agriculture and mining. The Witwatersrand Basin is well known for its extensive gold and uranium mining (Abiye et al., 2011), while there is also economically exploitable coal (DWA, 2013). Additionally, there is large-scale urbanisation and industrial activities in the basin (Abiye et al., 2011). Mining consequences, specifically acid mine drainage (AMD) from flooding of old mines in the Witwatersrand Basin, have been regarded as a major threat, mostly to shallow groundwater resources that are used for human supply and agricultural activities (Coetzee et al., 2010).

The Eastern Basin of the Witwatersrand Goldfields' study area has several sills and dykes, such as the Green Syenite Sill and the Modder East Dyke, which passes beneath the Cowles Dam (Scott et al., 1993). The Green Syenite Sill controls the groundwater flow direction and acts as a possible boundary to vertical groundwater flow. The occurrence of dykes, along with sills and chert layers, further divides the karstic dolomites into distinct hydrogeological compartments (Scott, 1995; Lea et al., 2003) with one such compartment assumed to exist around Enstra (Scott et al., 1993). The occurrence of these multiple geological structures may lead to the complexity of a hydrogeological system. In such a complex geology and structurally controlled area, the groundwater composition might be affected by different hydrogeochemical processes or other factors. An area like the Eastern Basin, which is exposed to various water-threatening human activities, may also be influenced by anthropogenic activities.

Several studies have addressed groundwater chemistry related to mining activities, aquifer vulnerability, and karst aquifer dewatering in the Witwatersrand Goldfields (DWA, 2013; Abiye et al., 2011; Schrader, 2015; Schrader and Winde, 2015). However, detailed studies on factors that influence the groundwater chemistry in the complex hydrogeological setting of the Witwatersrand Goldfields are limited. Mokadem et al. (2021) detailed hydrogeochemical processes and anthropogenic activities

that affect karst aquifers in the Far West Rand Basin. The present study is aimed at assessing factors influencing the groundwater quality in the Eastern Basin, an area whose hydrogeology is controlled by geological structures which act as groundwater flow boundaries. This study further assessed the suitability of groundwater quality for domestic and irrigation use purposes. The study used hydrochemical facies, principal component analysis (PCA), bivariate correlation plots, saturation indices, and Cl/Br mass ratios to understand the dynamics that are associated with groundwater chemistry evolution to enhance groundwater resource protection and sustainable management.

STUDY AREA

The Witwatersrand Goldfield is the largest in the world and has yielded more than one-third of all the gold ever produced on Earth (Tucker et al., 2016). While much of the basin is hidden under younger cover rocks, the gold-bearing conglomerates outcrop in the three oldest mining districts, namely, the West Rand, Central Rand, and East Rand Goldfields (McCarthy, 2006). Due to the interconnection of the underground workings within each of these goldfields, they are often referred to as the Western, Central and Eastern Basins. The current study was conducted in the Eastern Basin, as illustrated in Fig. 1.

Groundwater samples were collected from boreholes as marked in Fig. 1a, near the Alexander and Cowles Dams. Both the Cowles and Alexander Dams were in the early days of mining mainly used as sources of freshwater supply to the mining area. Cowles Dam is located near paper manufacturing plants, while to the south of these plants there is a solid waste disposal site and a sewage disposal works (Fig. 1a). The area is also characterised by mining and agricultural activities and residential areas.

The Witwatersrand Basin is almost entirely overlain by the Karoo and Transvaal sediments in the East Rand region, with outcrop areas of Witwatersrand strata limited to the northwestern and extreme southern part of the Goldfield (Fig. 2) (McCarthy, 2006; Scott, 1995). The rocks associated with the Karoo Supergroup, especially in the Eastern Basin, are sandstone, shale, coal seams, and diamictite, whereas those associated with the Transvaal are dolomite, chert, shale, limestone, quartzite, and subordinate conglomerate. The area is further intruded by dykes and sills of Karoo age, such as the Green Syenite Sill and the Modder East Dyke (Scott et al., 1993).

There are two main karst aquifers identified in the Eastern Basin, with yields ranging from 2 to 5 L/s (Fig. 1b). Scott (1995) stated that one of these aquifers lies on the Witwatersrand sediments and includes sills that intrude on the sediments. The sills in these dolomites form perched aquifers with shallow water levels (Scott, 1995; Lea et al., 2003). A report by the Department of Water Affairs (DWA, 2013) explained that the occurrence of perched aquifers is mainly in the mined-out coal zones and sandstones. According to Scott (1995), the second dolomite aquifer overlies the Ventersdorp Supergroup rocks, and is described as highly fractured and faulted. In this aquifer, geological structures act as flow paths for groundwater from the karst features in the dolomite to the mine voids (Lea et al., 2003; DWA, 2013). However, dykes and sills in these aquifers may also act as barriers to the flow of groundwater (DWA, 2013).

METHODS

Groundwater sampling and chemical analysis

Figure 3 shows the rainfall patterns for 2019, 2020, 2024, and 2025, as obtained from the South African Weather Service (SAWS). This is the data that was recorded at the rainfall station (Station 0476399 0) at OR Tambo International Airport, South Africa, which happened to be the closest station with all the required data. Four groundwater sampling rounds were conducted in October/November 2019 (spring), February (summer) and October (spring) 2020, and June 2025 (winter). Sampling during the two spring seasons for the current study was associated with the onset of the rainfall season, which in most parts of South Africa occurs between October and November (Fig. 3). The average annual rainfall for 2019, 2020, and the first 5 months of 2025 was 61.2 mm, 57.5 mm, and 100.9 mm, respectively, with the highest rainfall received in January and February 2019, 2020, and 2025. In the months within which data collection was conducted, there was more rainfall in February 2025 (200.4 mm) than in the rest of the months.

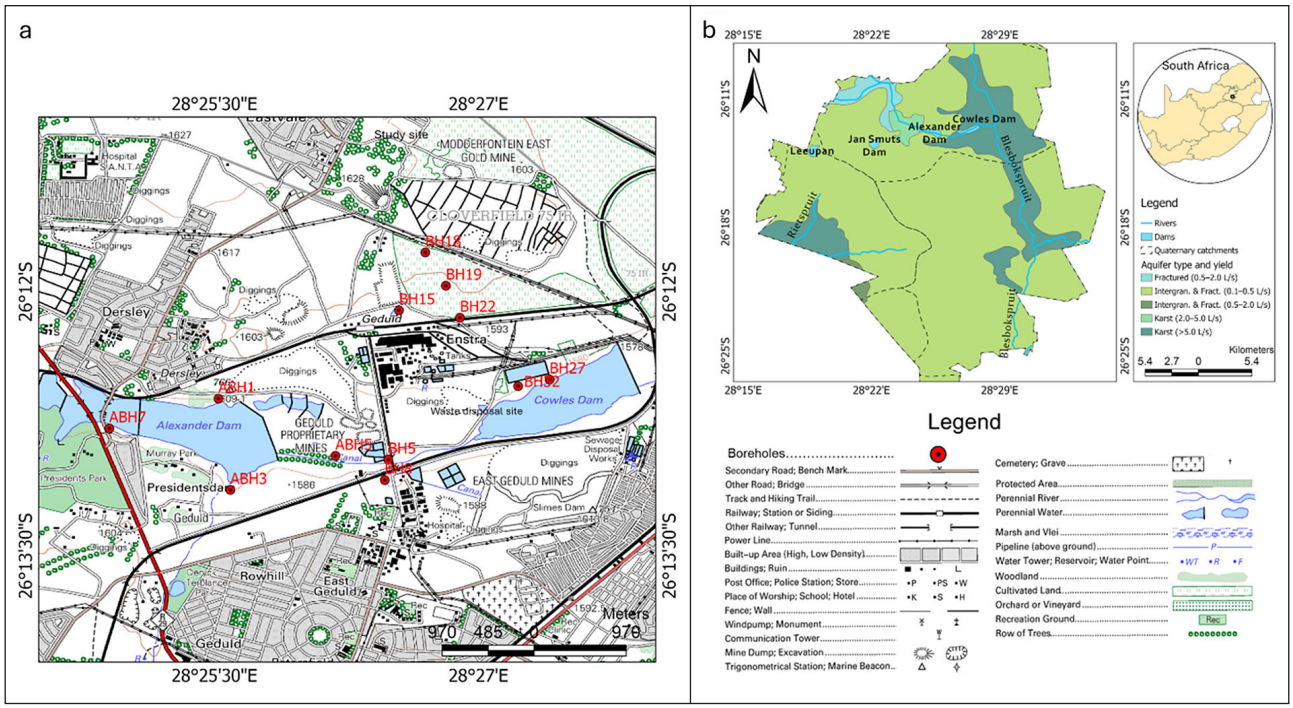

Figure 1. Map of the study area showing (a) sampled boreholes and (b) hydrogeological map of the Eastern Basin, Witwatersrand Goldfields

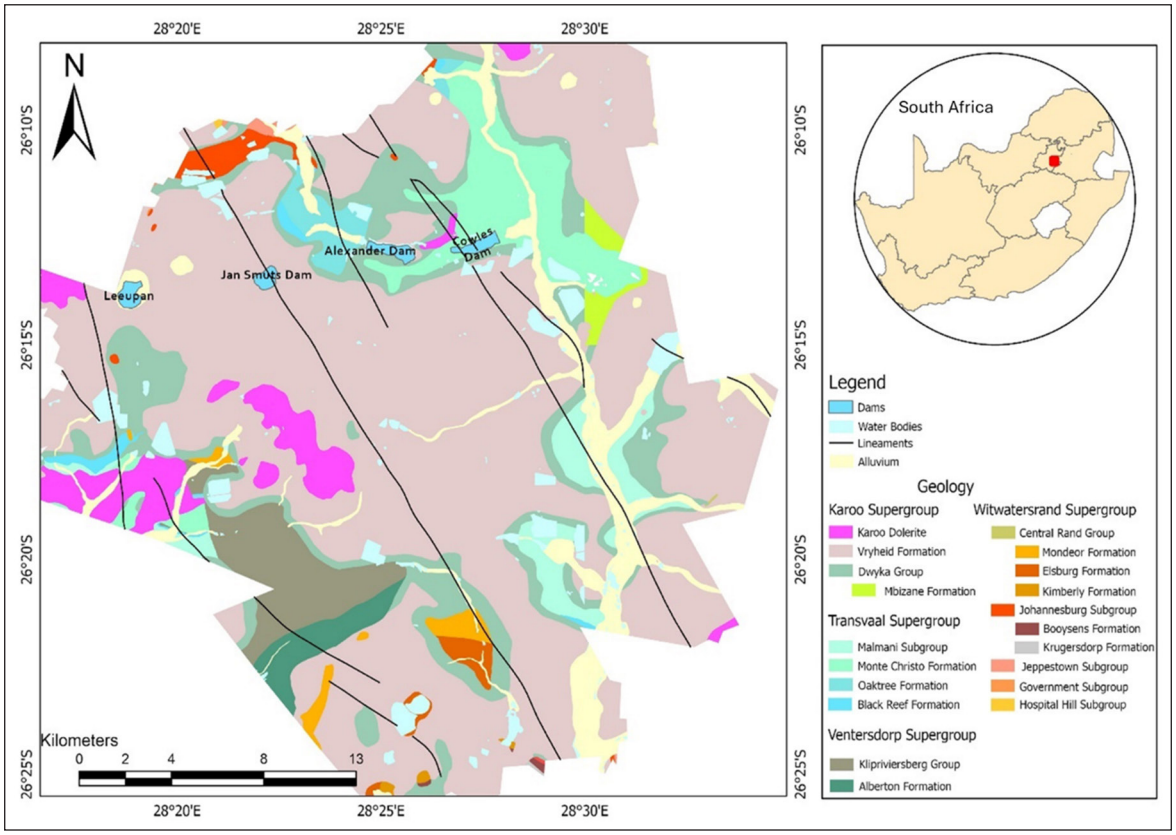

Figure 2. Geological map of the Eastern Basin, Witwatersrand Goldfields; and location within South Africa (inset)

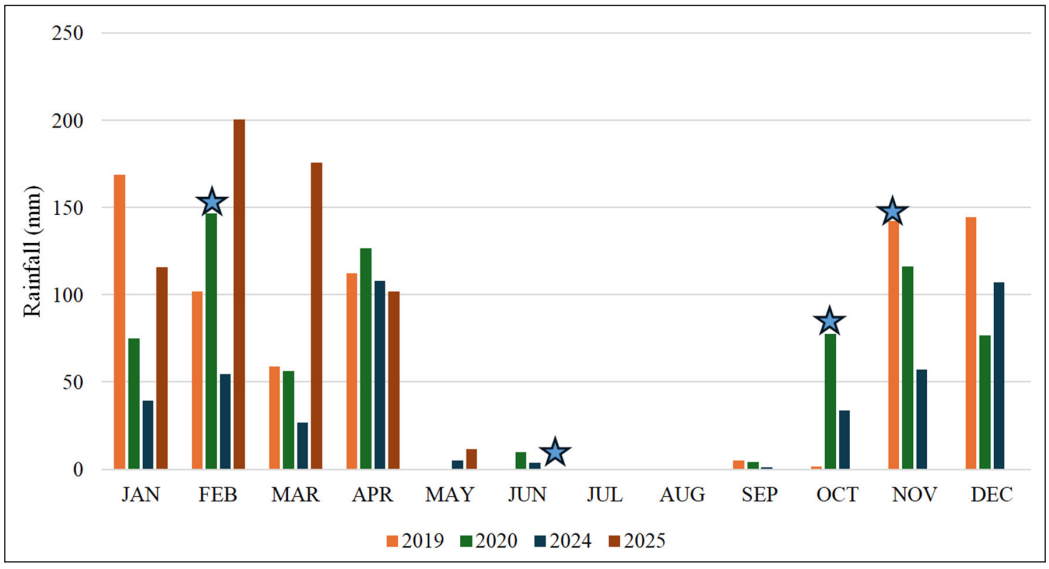

Figure 3. Rainfall data that were recorded at the OR Tambo rainfall station for the years 2019, 2020, 2024, and 2025, as obtained from SAWS. The star represents 4 sampling seasons.

A total of 12 boreholes, located northwest of Cowles Dam in the northern area and in the vicinity of the Alexander Dam in the southwestern area, were sampled (Fig. 1a, Fig. 4). During sampling in winter, only 8 boreholes were sampled, because the rest of the boreholes were either collapsed or vandalised. All the sampled boreholes are either used for monitoring the natural system or water quality at various facilities. Static water levels were measured using a dip meter from each borehole before the borehole water was disturbed. The water levels varied seasonally, with boreholes in the southwestern area indicating the effect of recharge on the water levels as observed for the winter and summer seasons. Less effect from recharge was observed on the groundwater in the northern area (Fig. 4).

Purging of the boreholes was done using plastic bailers to remove stagnant water before collecting a representative aquifer sample. To monitor if the bore well storage was removed, physico-chemical parameters such as electrical conductivity (EC), pH, redox potential (Eh), dissolved oxygen (DO), and temperature were measured using a Hanna multiparameter probe inside a closed probe tube. The volume of water to be removed from each borehole was not calculated; therefore, physico-chemical parameters were measured to test their stability, which led to the decision to collect the water samples (Barackman and Brusseau, 2002). According to Gomo et al. (2017), Eh and DO can still fluctuate slightly even after sufficient water has been removed through purging. Therefore, if pH, temperature, EC, and either Eh or DO are stable, sampling can then be conducted.

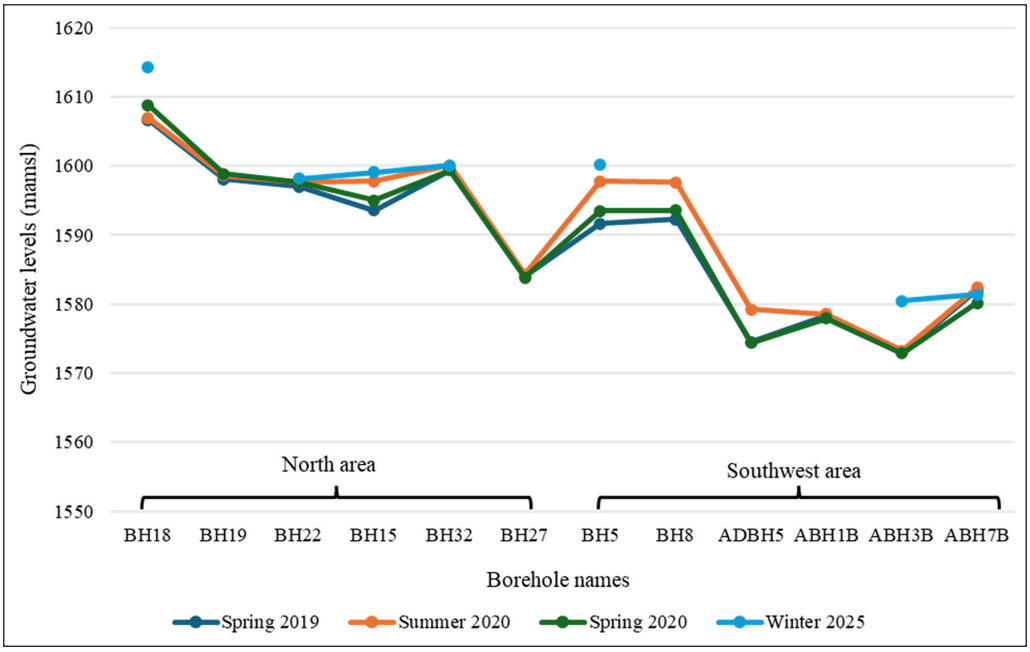

Figure 4. Groundwater levels measured during spring 2019 and 2020, summer, and winter seasons for the 12 boreholes in the north and southwest areas

Polyethylene plastic bottles with volumes of 100 mL and 500 mL were used to store water samples for inorganic chemical analyses. These bottles were new and only rinsed 3 times with the sample water before a sample was stored. Samples to be analysed for metals/metalloids were filtered (0.45 µm) and preserved by adding 3 drops of concentrated HNO_3, whilst unpreserved samples were collected for analyses of anions. Water samples were stored in portable ice chests that contained ice bricks and were transported to the laboratory for analysis after 4 days of sampling. Metals/metalloids and anions were analysed using inductively coupled plasma mass spectrometry and ion chromatography, respectively. The validity of the laboratory analysis was evaluated using the ion balance error (IBE). Most of the samples for all seasons measured ±10% IBE values, while BH32 had IBE values >10% for both spring and summer seasons. Other samples that measured high IBE were BH22 for the spring 2020 and BH18 for the winter seasons. The samples that measured >10% IBE were considered unreliable and not used for water quality interpretations, resulting in 11 samples considered during spring 2019 and summer seasons, and 10 for spring 2020. Only 7 boreholes were considered for winter data interpretations since 8 boreholes were sampled, and 1 had an IBE of >10%.

Data analysis and interpretation

A Piper trilinear diagram was used to group groundwater samples according to similar water types (Piper, 1944). The diagram was generated using the Geochemists' Workbench Software, while the sodium adsorption ratio (SAR) diagram was generated using the Windows Interpretation System for Hydrogeologists (WISH) program. The PCA was used as a tool to identify the factors that are responsible for the evolution of groundwater chemistry and was generated using the Statistical Package for Social Sciences (SPSS) software. Before generating the principal components, the data were standardised because they were measured using different scales. Equation 1, which calculates the z-score, was used to standardise the data.

$$Z = x\ (\text{value}) - \mu\ (\text{mean})/\sigma\ (\text{standard deviation}) \qquad (1)$$

The bivariate correlation plots, which were generated by Microsoft Excel, were used to correlate hydrochemical parameters to deduce hydrogeochemical processes that contributed to the groundwater chemistry change. The saturation indices (SI) were computed by the pH reaction equilibrium calculation (PHREEQC) hydrogeochemical program and were used to assess the saturation state of groundwater concerning carbonates (calcite and dolomite), halite and gypsum. According to Parkhurst and Appelo (1999), if minerals are saturated or have reached equilibrium conditions in solution, the SI value will be zero (0), whereas if a mineral is undersaturated, SI will be <0, while if supersaturated or oversaturated, the SI value will be >0. Parkhurst and Appelo (1999) further explained that the direction of the specific process taking place within the system is shown by the saturation state of minerals relative to the water. Thus, for all the minerals that show undersaturation concerning water, their dissolution will be anticipated, whereas for those that are supersaturated, their precipitation will be expected. The Cl/Br mass ratio was used as a tool to assess anthropogenic contamination in the groundwater (Katz et al., 2011).

RESULTS AND DISCUSSION

Hydrochemical parameters

The descriptive statistics for the hydrochemical parameters are displayed in Table 1. These concentrations were calculated for groundwater samples for the spring (2019 and 2020), summer and winter seasons. The EC values in the groundwater ranged between 394 µS/cm and 11 990 µS/cm for spring 2019, 395 µS/cm and 6 120 µS/cm for summer, 116 µS/cm and 3 580 µS/cm for spring 2020, and 326 µS/cm and 6 008 µS/cm for winter seasons.

The highest ECs were measured in groundwater samples collected from the northern area, northwest of Cowles Dam, particularly BH15, while in the southwestern area, high levels were measured from ABH3B groundwater for all seasons. A general observation is that EC was lower in most groundwater during the spring 2020 season, and below the recommended drinking water standard of 1 700 µS/cm by the South African Bureau of Standards (SABS, 2015). The groundwater in the area had, on average, circumneutral pH values ranging between 6.5 and 9.6. Iron and Mn displayed maximum concentrations of 25.6 mg/L and 23.5 mg/L in spring 2019, 21.3 mg/L and 1.3 mg/L in summer, 21.8 mg/L and 1.6 mg/L in spring 2020, and 0.005 mg/L and 3.8 mg/L in winter seasons, respectively (Table 1). The highest Fe concentrations were measured in some groundwater samples collected from the southwestern area.

Table 1. Descriptive statistics showing minimum, maximum, and mean values for hydrochemical parameters and reference drinking water standards for samples collected during the spring 2019, summer 2020, spring 2020, and winter 2025 seasons

Parameters	Spring 2019			Summer 2020			Spring 2020			Winter 2025			Recommended standards	
	Min.	Max.	Mean	Min.	Max.	Mean	Min.	Max.	Mean	Min.	Max.	Mean	SANS (2015)	WHO (2022)
pH	6.5	9	7.5	6.8	9.6	7.7	6.9	8.4	7.6	6.7	9.1	7.9	≥5≤9.7	6.5–8.5
EC (µS/cm)	394	11 990	2 298	395	6 120	1 485	116	3 580	758	326	6 008	2 133	1 700	3 000
Calcium (mg/L)	3.5	285.5	71.8	3.5	192	45.3	5	162	50.5	2.4	210	57.7	ND	ND
Magnesium (mg/L)	5	179.5	65.6	14.9	181	71.9	8.7	202	77.7	5.3	173	67.6	ND	ND
Sodium (mg/L)	25.5	3612	395.1	27	3 170	369	32.9	288	103	63.6	1 628	324.1	≤200	200
Potassium (mg/L)	2.1	33.2	10.6	2.9	39.8	12.2	2.6	38.9	12.4	2.3	13.5	7.7	ND	ND
Alkalinity as HCO_3 (mg/L)	72.2	7 286	924	59	4 448.9	599.2	24.7	385	185.2	32.2	2 915	642	ND	ND
Chloride (mg/L)	50	553.5	188.8	8.3	375.3	137.7	41.2	406.4	142.3	38.8	739	261.4	≤300	250
Sulphate (mg/L)	2	1 715.5	340.4	5	1 348.1	314.9	1.1	1 110.1	285.9	1	760	243	≤250	250
Nitrate as NO_3 (mg/L)	0.1	12.5	1.4	0.7	35.7	4	0.5	4	1.5	0.1	3.3	0.6	≤11	50
Bromide (mg/L)	NM	NM	NM	0.7	2.1	0.96	0.07	2.7	1.2	NM	NM	NM	ND	0.5
Iron (mg/L)	0.06	25.6	4.7	0.04	21.3	4.7	0.04	21.8	3	0.005	0.005	0.005	<2	0.3
Manganese (mg/L)	0.03	23.5	3	0.01	1.3	0.4	0.04	1.6	0.4	0.001	3.8	0.6	<0.4	0.02

ND – not defined; NM – not measured

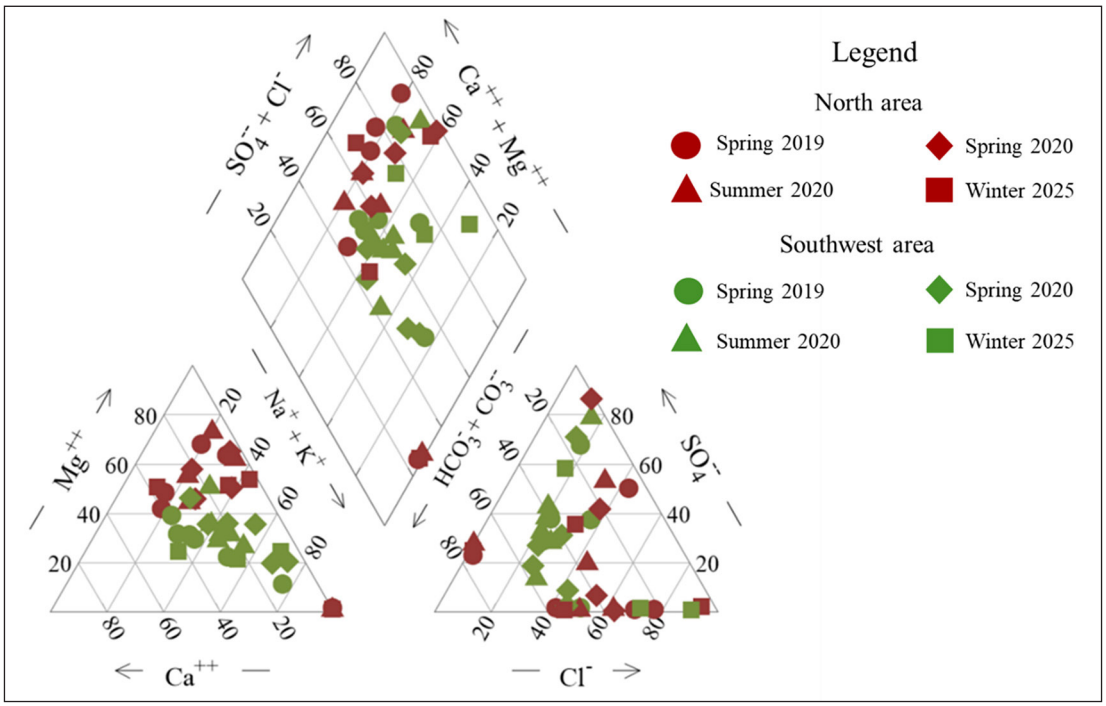

Figure 5. Piper diagram displaying groundwater samples collected from the northern and southwestern areas during spring 2019 and 2020, summer 2020, and winter 2025

The concentrations of Ca^{2+} in the groundwater ranged from 3.5 mg/L to 285.5 mg/L in spring 2019, 3.5 mg/L to 192 mg/L in summer, 5 mg/L to 162 mg/L in spring 2020, and 2.4 mg/L to 210 mg/L in winter. Magnesium ranged from 5 mg/L to 179.5 mg/L, 14.9 mg/L to 181 mg/L,8.7 mg/L to 202 mg/L, and 5.3 mg/L to 173 mg/L, while Na^+ concentration ranged from 25.5 mg/L to 3 612 mg/L, 27 mg/L to 3 170 mg/L, 32.9 mg/L to 288 mg/L, and 63.6 mg/L to 1 628 mg/L for spring 2019, summer, spring 2020, and winter seasons, respectively. Alkalinity as HCO_3^-, SO_4^{2-} and Cl^- had concentrations ranging from 72.2 mg/L to 7 286 mg/L, 2 mg/L to 1 715 mg/L, and 50 mg/L to 553.5 mg/L in spring 2019, 59 mg/L to 4 448 mg/L, 5 mg/L to 1 348 mg/L, and 8.3 mg/L to 375 mg/L in summer, 24.7 mg/L to 385 mg/L, 1.1 mg/L to 1 110.1 mg/L, and 41.2 mg/L to 406.4 mg/L in spring 2020, and 32.2 mg/L to 2 915 mg/L, 1 mg/L to 760 mg/L, and 38.8 mg/L to 739 mg/L in winter, respectively (Table 1). The dominance in the major ions varied considerably from site to site, with groundwater in the northern area mostly dominated by Mg^{2+}, Cl^-, and SO_4^{2-}. The maximum NO_3^- concentration was 35.7 mg/L, which was measured from one groundwater sample during the summer season. Otherwise, NO_3^- was <11 mg/L, which is the standard stipulated by SANS (SABS, 2015).

Hydrochemical facies

Piper diagrams were used to assess the main water types in the study area (Fig. 5). The southwestern area groundwater evolved from a recently recharged $CaHCO_3$ water type in some groundwater during spring 2019 to a mixed species, which was dominated by Na^+ and HCO_3^- ions during the other seasons except for winter, which produced $CaNaSO_4$ and NaCl water types.

Borehole ABH3B, which is located downgradient in the southwestern area, was also an exception and yielded a $MgSO_4$ water type during the different seasons, except in winter, where the water was NaCl. Groundwater from the northern area, on the other hand, was dominated by Mg^{2+} and Cl^- and/or HCO_3^- or SO_4^{2-} for all seasons, yielding a MgCl / $MgClSO_4$ / $MgClHCO_3$ water type (Fig. 5). The chemical composition of groundwater from BH15 (northern area) was $NaHCO_3$ during all seasons except spring 2020, when this was $MgSO_4$.

Hydrogeochemical processes

Naturally, fresh recharged water mineralises along the flow paths from the recharge to discharge areas due to the accumulation of ions during rock–water interactions (Pawar, 1993). To better understand the hydrogeochemical processes that control the evolution of groundwater chemistry, bivariate correlation plots, SI and PCA were evaluated.

Silicate weathering

Silicate weathering is an important process responsible for the evolution of groundwater chemical composition, often resulting in high Na^+ or Ca^{2+} concentrations. The Na^+/Cl^- molar ratio for the southwestern area groundwater was >1 (Fig. 6a), suggesting additional sources of Na^+ other than halite (molar ratio = 1) and likely due to silicate weathering (Meyback, 1987).

Rajmohan and Elango (2004) explained that if Na^+ comes from silicate weathering, HCO_3^- will be the dominant anion in the water. The reason HCO_3^- will be the dominant anion is that when feldspars react with carbonic acid in the presence of water, they release HCO_3^- (Elango et al., 2003), as shown by Eq. 2.

$$NaAlSi_3O_8 + 4.5H_2O + H_2CO_3 \rightarrow Na^+ + HCO_3^- + 0.5Al_2Si_2O_5(OH)_4 + 2H_4SiO_4 \quad (2)$$

This was observed in the southwestern area groundwater, which yielded a mixed groundwater facie dominated by Na^+ and HCO_3^- during the different seasons (Fig. 5). This mixed water type may be associated with natural processes such as ion exchange. Since the Karoo sediments cover a large portion of the Eastern Basin, Na^+ from these sediments could be altering the water composition with time as it travels along the flow path by replacing Ca^{2+} through cation exchange (Ligavha-Mbelengwa and Gomo, 2020), hence the chemistry of the water evolved from $CaHCO_3$ to $NaHCO_3$. The effect of silicate weathering was also observed from the excess Na^+ over Ca^{2+} in most of the samples (Fig. 6b), which resulted from Ca^{2+} being exchanged for Na^+ from clay minerals (Pawar, 1993). Another likely possibility for the Na^+ dominance in the southwestern area groundwater could be that the water was influenced by anthropogenic activities where sodium-rich wastewater was released by industries or from agricultural contamination into the water systems (Vengosh and Keren, 1996). Considering various anthropogenic activities around the study area, this possibility cannot be entirely ruled out.

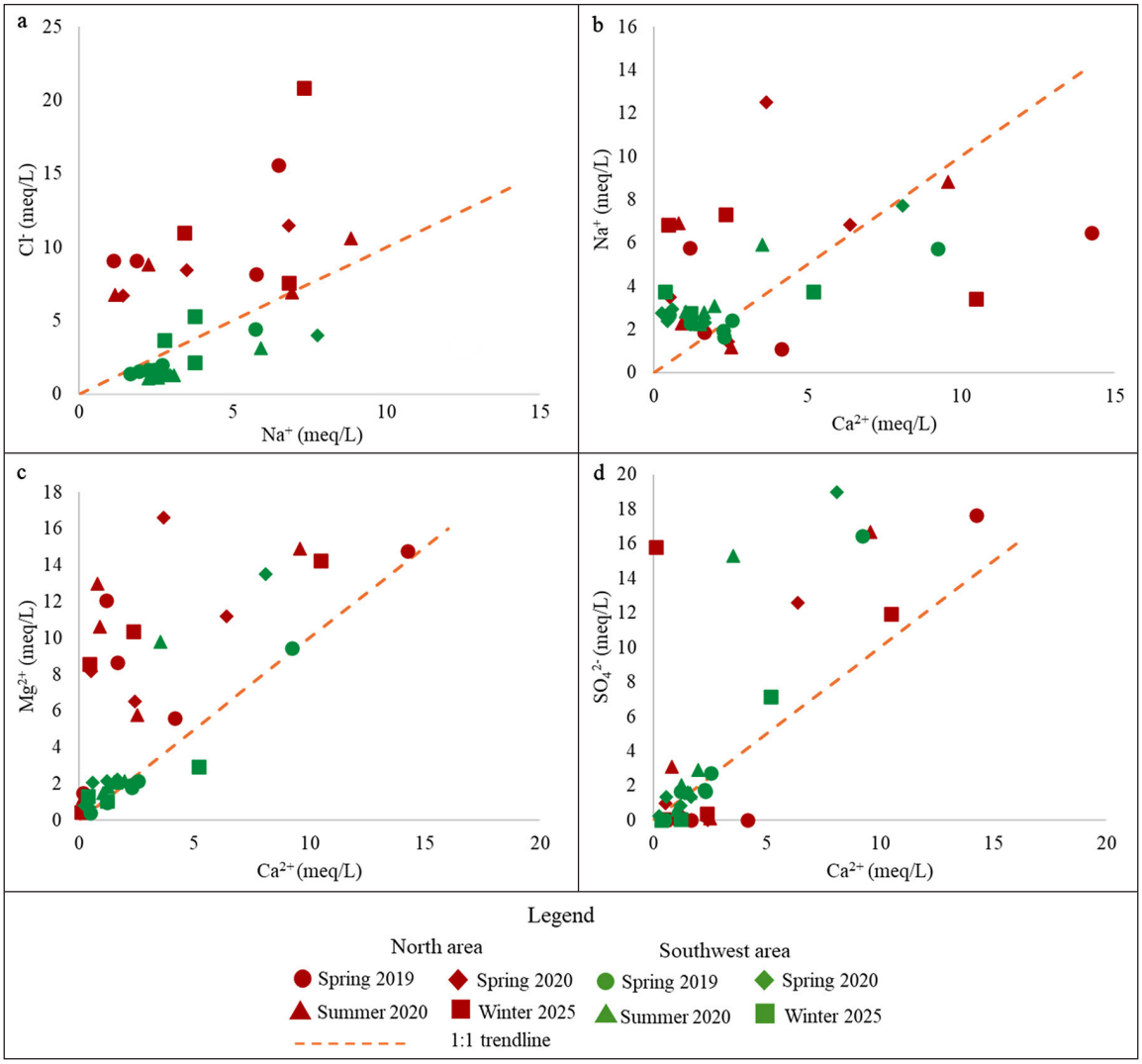

Figure 6. Bivariate correlation plots between hydrochemical parameters (a) Na^+ vs. Cl^-, (b) Ca^{2+} vs. Na^+, (c) Ca^{2+} vs. Mg^{2+}, and (d) Ca^{2+} vs. SO_4^{2-} for spring 2019 and 2020, summer, and winter sampling seasons. Sodium and SO_4^{2-} data from BH15 were excluded from the bivariate plots since these were outliers due to the highest concentrations.

An exception in the southwest area groundwater was observed for 2 samples during winter, as these reported Na^+/Cl^- molar ratios of <1, showing dominance in Cl^- (Fig. 6a). The SI_H values were <1 in all the samples, indicating that groundwater was undersaturated in halite mineral. Thus, the excess Cl^- in these samples could be attributed to anthropogenic contributions during recharge in winter. This is especially because Cl^- concentrations in surface water, as associated with prolonged rainfall, were less (<60 mg/L) in winter; also, Cl^- was generally low in the groundwater samples during the three prior sampling periods. The high Cl^- could have emerged through other preferential flow paths.

The northern area groundwater also produced Na^+/Cl^- ratios <1 during all seasons (Fig. 6a). This suggests that groundwater was influenced by other chemical processes than silicate weathering (Rajmohan and Elango, 2004).

Dissolution and precipitation

The presence of minerals such as calcite and dolomite in equilibrium with groundwater indicates that these minerals are reactive and influence the solution concentrations under normal groundwater environments (Rajmohan and Elango, 2004). The SI produced values >1 for calcite (SI_C) and dolomite (SI_D) in most of the samples from the northern area, and a few in the southwestern area (Table A1), indicating water that is supersaturated with these minerals.

Generally, the SI_D values were higher than the SI_C values in all samples, possibly suggesting that during calcite precipitation, silicate weathering contributed Mg^{2+} and Na^+ into the solution (Pawar, 1993). The supersaturation of groundwater in dolomite corresponds with the Ca^{2+}/Mg^{2+} ratios of 1 or less, suggesting additional Mg^{2+} in solution (Fig. 6c). The overall observation with the Ca^{2+}/Mg^{2+} ratios, SI_D and SI_C values indicates that the process of carbonate dissolution influenced both the northern and southwestern areas' groundwater, although at different rates. This was more evident in the northern area groundwater, which was dominated by Mg^{2+} cation, and in other cases, HCO_3^- anion. According to Mayo and Loucks (1995), a Ca^{2+}/Mg^{2+} ratio of 1 or less indicates dolomite dissolution, while a ratio between 1 and 2 represents calcite dissolution, and a ratio > 2 suggests silicate weathering. Some of the Mg^{2+} in solution, as shown by a Ca^{2+}/Mg^{2+} ratio <1, could have been added through mineral exchange when sodium-rich feldspar dissolved from silicates (Jalali, 2007).

The supersaturation of the northern area groundwater with calcite and dolomite, even after recharge in summer and winter seasons, implies that the aquifer is large and experiences less effect from dilution during recharge, as also indicated by minor groundwater level changes during the seasonal transition (Fig. 4), whereas the undersaturation in the southwestern area groundwater could indicate the effect of dilution from recharge on the groundwater composition. This agrees with observations made by Rajmohan and Elango (2004), who noted undersaturation of calcite and dolomite in groundwater during the wet season because of dilution.

The process of gypsum dissolution was deduced from the Ca^{2+}/SO_4^{2-} molar ratios of 1 or approximately 1, as another hydrogeochemical process influencing groundwater in the southwestern area, with some samples plotting on or closer to the 1:1 line (Fig. 6d). This process generally contributed Ca^{2+} and SO_4^{2-} ions to the groundwater. However, all the groundwater samples were undersaturated with gypsum (SI_G) during all seasons, with SI_G values of <1, (Table A1). This suggested that although gypsum dissolution potentially influenced the groundwater composition, this mineral did not reach equilibrium conditions (Parkhurst and Appelo, 1999). Thus, the additional Ca^{2+} that led to some samples plotting below the 1:1 line emerges from carbonate dissolution as outlined, while the excess SO_4^{2-} in some groundwater, especially in the north, is associated with anthropogenic activities (Mokadem et al., 2021).

Ion exchange and reverse ion exchange

Ion exchange occurs when Ca^{2+} ions are removed from groundwater to replace the void spaces in the sediments. This process can be illustrated through bivariate correlation graphs of Na^+ vs. Cl^- (Fig. 6a) or $Ca^{2+}+Mg^{2+}$-SO_4^{2-}-HCO_3^- vs. Na^+-Cl^- (Jankowski and Beck, 2000). When subtracting Cl^- from Na^+, with an assumption that all Cl^- originated from precipitation, groundwater that is not affected by ion exchange will plot close to zero on the Na^+-Cl^- axis. Similarly, when SO_4^{2-} and HCO_3^- are subtracted from Ca^{2+} and Mg^{2+}, the dissolution of calcite, dolomite, and gypsum should also return to zero values if dissolution occurs at the same rate and no ion exchange takes place (Jankowski and Beck, 2000). However, if ion exchange is the dominant process, groundwater samples will plot on a straight line with a slope of −1 (Fig. 7a). Ion exchange and reverse ion exchange are expressed as Eq. 3 and Eq. 4, respectively, with X representing the exchange site (Fisher and Mullican, 1997).

$$2Na^+ + CaX_2 \rightarrow 2NaX + Ca^{2+} \quad (3)$$

$$Ca^{2+} + 2NaX \rightarrow CaX_2 + 2Na^+ \quad (4)$$

The groundwater samples from the southwestern area plots below the 1:1 line for different seasons, showing dominance in Na^+, further indicating that this water was predominantly influenced by ion exchange (Fig. 6a). Additionally, in Fig. 7a, these groundwater samples plot close to a line ($r = 0.8$) with a slope of −0.77, which is close to −1. This further validates the process of ion exchange, where Ca^{2+} was replaced by Na^+ in the groundwater (Jalali, 2007), resulting in the mixed water type dominated by Na^+ and HCO_3^-.

The graph of $Ca^{2+}+ Mg^{2+} - SO_4^{2-} - HCO_3^-$ vs. $Na^+ - Cl^-$ for northern area groundwater also produced a gradient of −0.64 (Fig. 7b), which supports the process of ion exchange. By contrast, in Fig. 6a, the northern area samples are plotted above the 1:1 trendline, showing excess Cl^-, which opposes ion exchange as a composition controlling process. The observation in Fig. 7b could suggest that the northern area groundwater was influenced by both ion exchange and dolomite dissolution, as supported by the Ca^{2+}/Mg^{2+} ratio of 1 or less (Fig. 6c) and oversaturation of dolomite and calcite in this groundwater. This observation shows that excess Cl^- could be emerging from anthropogenic activities. This is because the SI as presented in Table A1 showed $SI_H < 0$, indicating that all the groundwater in the area is undersaturated in halite. This means that halite dissolution is not the cause of high Cl^- in solution, since this mineral was not in equilibrium with the groundwater (Parkhurst and Appelo, 1999). The study area, especially in the northern area, is characterised by various industrial activities and mine tailings processing that may contribute to contamination of groundwater.

Natural and anthropogenic influence

Principal component analysis was used as a complementary tool to illustrate factors controlling the groundwater composition and to differentiate between groundwater influenced by natural processes and that influenced by anthropogenic activities.

The cumulative variance for the 2 components of the southwestern area groundwater was ~70%. Component 1 was represented by high positive loadings of EC, Ca^{2+}, Mg^{2+}, Na^{2+}, Cl^-, and SO_4^{2-} (Fig. 8a).

These high loadings of major ions and EC are associated with mineralisation by rock–water interaction as the main process that influenced the groundwater composition in the southwestern area. This supports what has been deduced from hydrogeochemical processes that the southwestern area groundwater chemistry

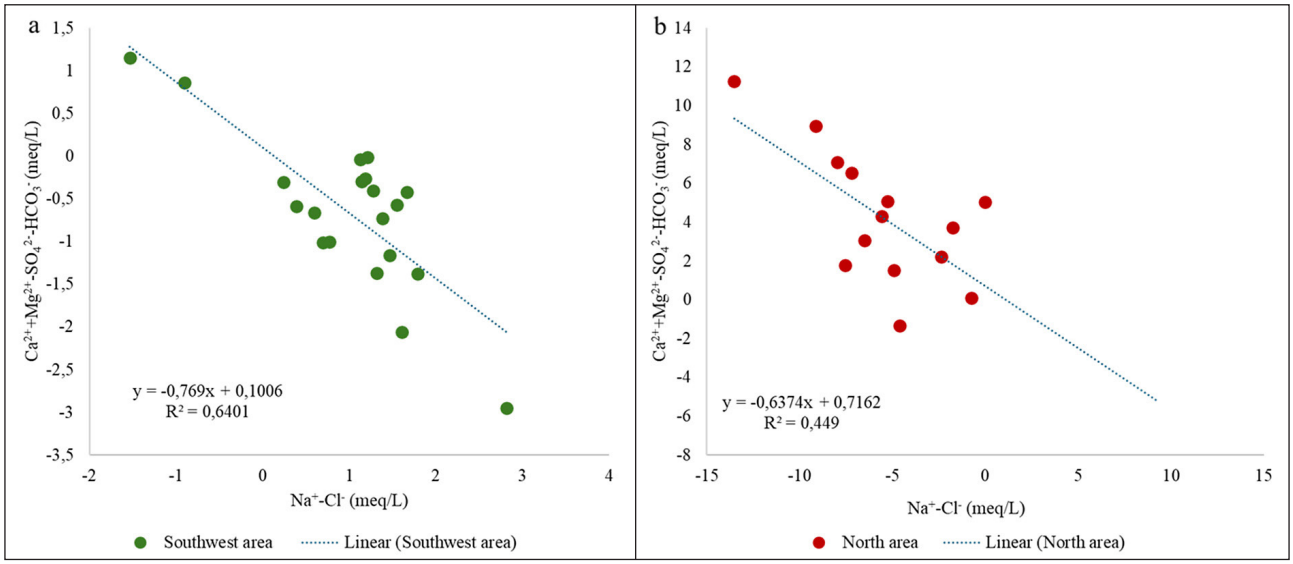

Figure 7. Bivariate correlation plots between hydrochemical parameters $Ca^{2+} + Mg^{2+} - SO_4^{2-} - HCO_3^-$ vs. $Na^+ - Cl^-$ for the (a) western area groundwater and (b) northern area groundwater

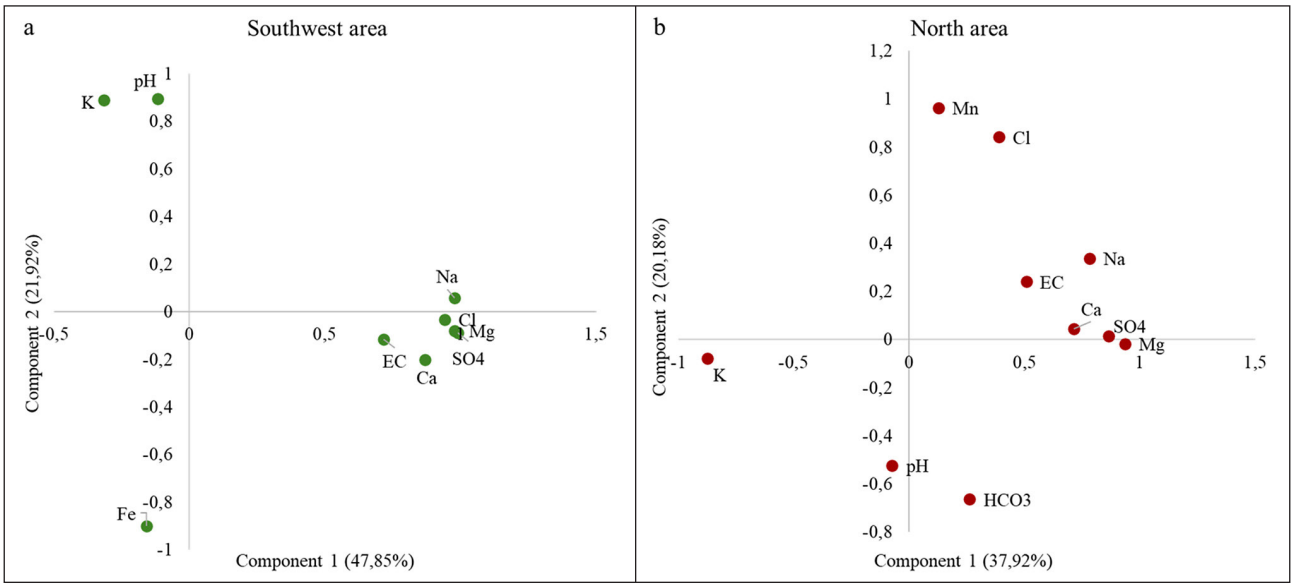

Figure 8. PCA plots in rotated space for Components 1 and 2 for the different seasons in the (a) southwestern area and (b) northern area groundwater

was influenced by silicate weathering, ion exchange, carbonate and gypsum dissolution. The process of rock–water interaction is often dependent on pH. The low negative loading of pH under Component 1 indicated that mineralisation increases with a decrease in pH.

The correlations between pH and K^+ in Component 2 were high (Fig. 8a) in the southwestern area groundwater. Although there is no defined South African National Standard (SANS) for drinking water for K^+, the concentrations reported for the southwestern area groundwater were <13 mg/L. Thus, the positive loadings of pH and K^+ could suggest that as the pH levels increase, K^+ is released into the groundwater, leading to its high concentrations.

Although negative, the loading of Fe was high under Component 2, displaying an inverse relationship against pH. The Fe concentrations in the southwestern area groundwater reported an average of 5.6 mg/L and a maximum of 25.6 mg/L, which exceeds the 2 mg/L standard as recommended by the SABS (2015) (Table 1). The high Fe concentrations in some of the southwestern area groundwater did not correspond with either EC or SO_4^{2-} to indicate the influence of groundwater by mining activities. The average SO_4^{2-} concentration in the southwestern area groundwater was 179.3 mg/L, while the EC was 558 µS/cm. According to Gray (1996), SO_4^{2-} and EC are the best indicators of AMD contamination because, unlike pH, these are sensitive to AMD even when there is dilution. Abiye et al. (2011) have reported average SO_4^{2-} concentrations of 3 500 mg/L and Fe concentrations of 300 mg/L for groundwater that was affected by AMD in the Johannesburg area, Witwatersrand Basin. The average SO_4^{2-} in water that was not affected by AMD in their study was <40 mg/L. The average concentrations of AMD-influenced groundwater were way higher than what was reported in the current study, which was conducted in the same region. Research by the Council for Geoscience (Madzivire et al., 2022) also showed that groundwater monitoring in this area has not revealed major groundwater contamination related to mining activities. Therefore, despite the mining history that contributed to AMD contamination in water resources around the Witwatersrand Basin (Abiye et al., 2011; DWA, 2013), the presence of Fe in the groundwater of the study area does not support possible influence by mining activities. The high Fe concentrations could be due to corrosion of the steel casings used during borehole construction.

The cumulative variance for the 2 components of northern area groundwater accounted for 58% in the different seasons. The northern area groundwater also produced high positive loadings of EC, Na^+, Ca^{2+}, Mg^{2+}, and SO_4^{2-} grouped together under Component 1, alluding to mineralisation by rock–water interaction as one process that influenced the composition of this water, as supported by the deductions from the hydrogeochemical processes (Fig. 8b). The excess Cl^- that resulted in MgCl / $MgClSO_4$ / $MgClHCO_3$ water types produced a high positive loading under Component 2. This indicates that, unlike the other major ions under Component 1, Cl^- contribution was not due to mineralisation, but a different process which is likely anthropogenic activities as validated by Na^+/Cl^- ratios <1 and undersaturated SI_H values.

The groundwater from the northern area also reported higher EC values (average = 2 910 µS/cm), as opposed to the average of 558 µS/cm that was reported for groundwater in the southwestern area. Although EC is an indirect indicator of contamination because it is more closely related to the dissolved salt content in the water than it is associated with anthropogenic contamination (De Sousa et al., 2014), the excess Cl^- and, in some cases, SO_4^{2-} indicated anthropogenic influence particularly from industrial discharges and mine tailings processing, especially because these exceeded the 250 mg/L recommended by the World Health Organization (WHO, 2022).

The anthropogenic influence on the northern area groundwater was further corroborated by Cl/Br mass ratios >88 (Table A1). According to Alcalá and Custodio (2008), the Cl/Br mass ratio of 88–222 indicates contamination by agricultural activities, whereas a ratio between 300 and 600 represents wastewater contamination (Davis et al., 1998). Alcalá and Custodio (2008) further noted that the typical natural source of Cl^- is halite, which gives Cl/Br ratios of up to 1 200, while anthropogenic sources will lower the ratio.

Water quality assessments

Water suitability for domestic purposes

The water quality was assessed for its suitability for domestic and agricultural purposes, using the drinking water quality guidelines reported by the SABS (2015) and the World Health Organization (WHO, 2022). The evaluation also included the total hardness (Eq. 5) for determining the water's suitability for domestic use. M^{2+} in Eq. 5 represents divalent cations of Ca^{2+} and Mg^{2+}, which and are reported in mg/L.

$$\text{Hardness as } CaCO_3 = M^{2+}\left(\frac{\text{Equivalent weight of } CaCO_3}{\text{Equivalent weight of } M^{2+}}\right) \quad (5)$$

Northern area groundwater yielded very hard water, with a total hardness > 300 mg/L (DWAF, 1996) and was classified by a total dissolved solids (TDS) value that is 'fair' to 'unacceptable' for drinking purposes. Borehole BH15 was an exception in the northern area group since its hardness ranged from soft to moderately soft, although its TDS was 'unacceptable'. Consequently, the southwestern area groundwater, except ABH3B, yielded water that ranged between soft and hard (Table 2), while the TDS indicated that this water is good for domestic purposes (WHO, 2022), since it was below 600 mg/L (Table 3). Groundwater from ABH3B was very hard and thus classified as 'unacceptable' for use.

Water suitability for irrigation purposes

The water quality was also assessed for irrigation suitability by calculating the salinity and alkalinity hazards (Eq. 6), sodium percentage (Na%) (Eq. 7) and residual sodium carbonate (Eq. 8). The ion concentrations used in these equations are in meq/L.

$$SAR = \frac{Na^+}{\sqrt{\frac{Ca^{2+} + Mg^{2+}}{2}}} \quad (6)$$

$$Na\% = \left(\frac{(Na^+ + K^+)}{(Ca^{2+} + Mg^{2+} + Na^+ + K^+)}\right) \times 100 \quad (7)$$

$$RSC = (HCO_3^- + CO_3^{2-}) - (Ca^{2+} + Mg^{2+}) \quad (8)$$

Salinity and alkalinity hazard

The total salt content of irrigation water is determined by the EC. The EC ranged from 39.4 mS/m to 1 199 mS/m, 39.5 mS/m to 612 mS/m, 11.6 mS/m to 358 mS/m, and 32.6 mS/m to 600 mS/m in the groundwater samples during spring 2019, summer 2020, spring 2020, and winter 2025 seasons, respectively. The salinity hazard in the southwestern groundwater area was classified as medium and low salinity hazard during the different seasons, except in ABH3B, which reported a high salinity (Fig. 9). Conversely, the northern groundwater area displayed a medium to very high salinity hazard.

Table 2. Total hardness of groundwater expressed as calcium carbonate (mg/L) (DWAF, 1996) for the spring 2019 and 2020, summer 2020, and winter 2025 seasons

Hardness range ($CaCO_3$ mg/L)	Hardness description	Number of boreholes			
		Spring 2019	Summer 2020	Spring 2020	Winter 2025
0–50	Soft	1[a]	0	0	1[b]
50–100	Moderately soft	1[b]	1[b]	2[a]	1[a]
100–150	Slightly hard	1[a]	1[a]	1[a]	1[a]
150–200	Moderately hard	0	3[a]	2[a]	0
200–300	Hard	4[a]	1[a]	0	0
>300	Very hard	4[b]	5 (1[a]; 4[b])	5[b]	4 (1[a]; 3[b])

[a]southwest area groundwater sample; [b]north area groundwater sample

Table 3. Groundwater quality classification concerning total dissolved solids (WHO, 2022) for the spring 2019 and 2020, summer 2020, and winter 2025 seasons

TDS range (mg/L)	Water class	Number of boreholes			
		Spring 2019	Summer 2020	Spring 2020	Winter 2025
<300	Excellent	2[a]	1[a]	2[a]	0
300–600	Good	3[a]	5 (4[a]; 1[b])	3[a]	2[a]
600–900	Fair	2[b]	1[b]	1[b]	1[a]
900–1 200	Poor	0	1[b]	1[b]	2[b]
>1 200	Unacceptable	4 (1[a]; 3[b])	3 (1[a]; 2[b])	3 (1[a]; 2[b])	2[b]

[a]southwest area groundwater sample; [b]north area groundwater sample

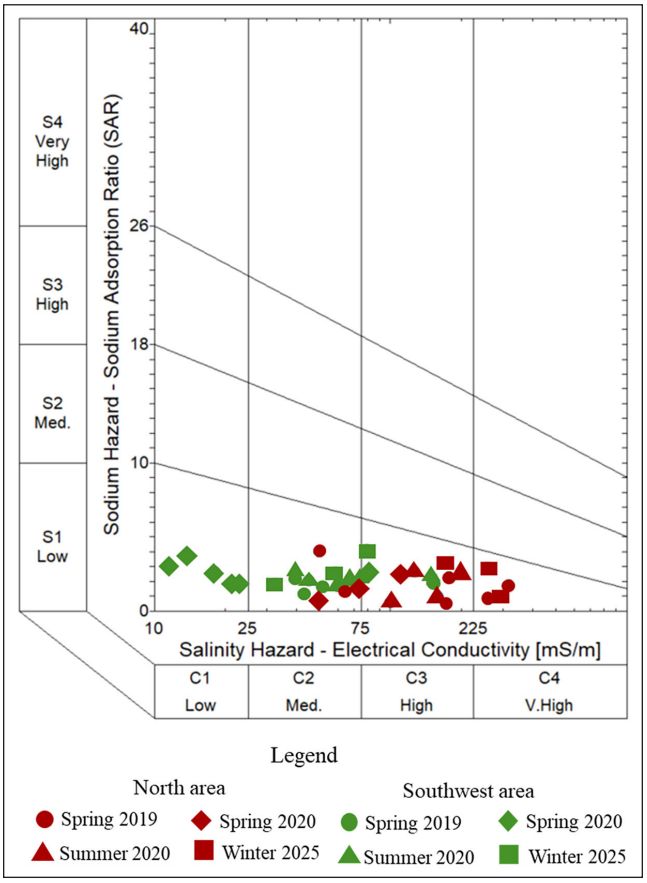

Figure 9. SAR diagrams classifying water for irrigation purposes for the spring 2019 and 2020, summer 2020, and winter 2025 seasons

Table 4. Groundwater quality assessment for irrigation uses for the spring 2019 and 2020, summer 2020, and winter 2025 seasons

Parameters	Range	Water class	Number of boreholes			
			Spring 2019	Summer 2020	Spring 2020	Winter 2025
SAR	<10	Excellent	10	10	10	6
	10–18	Good	0	0	0	0
	18–26	Doubtful	0	0	0	0
	>26	Unsuitable	1[b]	1[b]	0	1[b]
Na%	<20	Excellent	3[b]	0	0	1[b]
	20–40	Good	5 (4[a]; 1[b])	6 (2[a]; 4[b])	6 (2[a]; 4[b])	2 (1[a]; 1[b])
	40–60	Permissible	1[a]	4[a]	2[a]	2 (1[a]; 1[b])
	60–80	Doubtful	1[a]	0	2[a]	1[a]
	>80	Unsuitable	1[a]	1[b]	0	1[b]
RSC	<1.25	Safe	10	10	10	6
	1.25–2.5	Moderate	0	0	0	0
	>2.5	Unsuitable	1[b]	1[b]	0	1[b]

[a]southwest area groundwater sample; [b]north area groundwater sample

The groundwater can be used for irrigation with caution for crops that have a good salinity tolerance (DWAF, 1996). However, high salinity levels can negatively affect crop yields since this would lead to soil salinity.

The alkalinity hazard, often presented as SAR, is among the key parameters in assessing water suitability for irrigation (Wilcox, 1955). All the samples except BH15 had SAR values <10, indicating water that is excellent for irrigation. The samples from BH15 had SAR >130, classifying them as unsuitable for use. The southwestern area groundwater, except ABH3B, was categorised under the S1C2 and S1C1 classes for the different seasons (Fig. 9). This water was represented by low sodium and low to medium salinity, while the northern area groundwater fell within the S1C2, S1C3, and S1C4, revealing medium to very high salinity hazards (Fig. 9).

Sodium percentage (%)

Table 4 categorises most of the groundwater samples as 'good' to 'permissible' for irrigation purposes (Wilcox, 1955). Although a few samples, particularly in the southwestern area, are 'doubtful' or 'unsuitable' for use. Only samples from BH15 in the northern area yielded a Na% > 80, reporting water that is 'unsuitable' for irrigation.

Residual sodium carbonate

In the present study, the residual sodium carbonate (RSC) values were <1.25, showing water that is safe for irrigation usage (Table 4). This was except water from BH15 that had an RSC value >50, indicating water that is 'unsuitable' for irrigation use. According to Eaton (1950), water with RSC values of <1.25 is 'safe', 1.25 to 2.5 is 'moderate', and >2.5 is 'unsuitable' for irrigation purposes.

CONCLUSIONS

The study was aimed at evaluating factors that influence the groundwater chemical composition in a typical karst environment where the hydrogeology is controlled by geological structures. The findings revealed a hydrogeochemical distinction between groundwater in the southwestern and northern areas as follows:

- Groundwater in the southwestern area evolved from a $CaHCO_3$ type to a mixed facie dominated by Na^+ and HCO_3^- ions, while that in the northern area showed MgCl / $MgClSO_4$ / $MgClHCO_3$ water types.
- The main hydrogeochemical processes controlling groundwater chemistry in the southwestern area were silicate weathering, ion exchange, carbonate and gypsum dissolution
- The northern area was also controlled by hydrogeochemical processes, mainly carbonate dissolution. Although this groundwater was also largely influenced by anthropogenic activities, as proven by the Cl/Br mass ratios >88, excess Cl^- concentrations, and Cl^- clustering independently on the PCA. The Cl^- levels could not be attributed to halite dissolution, as halite was undersaturated in solution. Furthermore, this groundwater showed excess SO_4^{2-} which was associated with anthropogenic sources.
- Groundwater from the southwestern area was suitable for domestic use, while that from the northern area had very hard total hardness, classifying it as poor to unacceptable for domestic use. Groundwater from both aquifers was generally safe for irrigation purposes, except that from BH15.

The integrated application of hydrochemical tools served as a powerful approach which provided a better understanding of the dominant hydrogeochemical processes and anthropogenic factors influencing the groundwater quality. Furthermore, it provided a clear distinction between the northern and southwestern areas' groundwater, showing that these were influenced by different factors. This highlights the importance of developing area-specific protection and management strategies that consider both natural processes and anthropogenic impacts.

ACKNOWLEDGMENTS

The authors are grateful to the Mine Environment and Water Management Programme colleagues at the Council for Geoscience for contributing immensely to the task on which this piece of work was drawn. Enstra Paper in Springs and Mr Zietsman granted permission for data collection in and around their premises for the duration of this research, and for this the authors are grateful. The South African Weather Service provided all the weather data that were used in this research, which is greatly appreciated. The data contained in this research is published with permission granted by the Council for Geoscience. Dan Lapworth was supported by the BGS International NC programme 'Geoscience to tackle Global Environmental Challenges.' Dan Lapworth publishes with the permission of the Executive Director of the British Geological Survey.

This research was supported by the Council for Geoscience and the Department of Mineral Resources and Energy.

AUTHOR CONTRIBUTIONS

Conceptualisation, methodology, formal analysis, investigation, writing – original draft, writing – review and editing, visualisation: Lufuno Ligavha-Mbelengwa. Writing – review and editing, supervision: Modreck Gomo, Dan Lapworth and Godfrey Madzivire.

CONFLICTS OF INTEREST

One of the co-authors of this manuscript is a subject editor for *Water SA*.

ORCID

Lufuno Ligavha-Mbelengwa
https://orcid.org/0000-0003-3333-3322

REFERENCES

ABIYE TA, MENGISTU H and DEMLIE MB (2011) Groundwater resource in the crystalline rocks of the Johannesburg Area, South Africa. *J. Water Resour. Prot.* **3** 199–212. https://doi.org/10.4236/jwarp.2011.34026

ALCALÁ FJ and CUSTODIO E (2008) Using the Cl/Br ratio as a tracer to identify the origin of salinity in aquifers in Spain and Portugal. *J. Hydrol.* **359** (1–2) 189–207. https://doi.org/10.1016/j.jhydrol.2008.06.028

BARACKMAN M and BRUSSEAU ML (2002) Groundwater sampling. In: Janick FA, Pepper IL and Brusseau ML (Eds.) *Environmental Monitoring and Characterization*. Academic Press, Tucson, Arizona. 121–139. https://doi.org/10.1016/B978-012064477-3/50010-2

COETZEE H, HOBBS PJ, BURGESS JE, THOMAS A and KEET M (2010) Mine water management in the Witwatersrand Gold fields with special emphasis on acid mine drainage. Council for Geoscience, Pretoria.

DAVIS SN, WHITTEMORE DO and FABRYKA-MARTIN J (1998) Uses of chloride/bromide ratios in studies of potable water. *J. Groundw.* **36** (2) 338–350. https://doi.org/10.1111/j.1745-6584.1998.tb01099.x

DE SOUSA DNR, MOZETO AA, CARNEIRO RL and FADINI PS (2014) Electrical conductivity and emerging contaminant as markers of surface freshwater contamination by wastewater. *Sci. Total Environ.* **484** (1) 19–26. https://doi.org/10.1016/j.scitotenv.2014.02.135

DWA (Department of Water Affairs, South Africa) (2013) Feasibility study for a long-term solution to address the acid mine drainage associated with the East, Central and West Rand underground mining basins. DWA Report No. P RSA 000/00/16512/2. DWA, Pretoria.

DWAF (Department of Water Affairs and Forestry, South Africa) (DWAF) (1996) South African Water Quality Guidelines Agricultural Use: Irrigation. DWAF, Pretoria.

EATON FM (1950) Significance of carbonate in irrigation. *Water Soil Sci.* **67** 112–113.

ELANGO L, KANNAN R and SENTHIL KUMAR M (2003) Major ion chemistry and identification of hydrogeochemical processes of ground water in a part of Kancheepuram district, Tamil Nadu, India. *Environ. Geosci.* **10** (4) 157–166. https://doi.org/10.1306/eg100403011

FISHER RS and MULLICAN WF (1997) Hydrochemical evolution of sodium-sulfate and sodium-chloride groundwater beneath the Northern Chihuahuan Desert, Trans-Pecos, Texas, USA. *J. Hydrogeol.* **5** 4–16. https://doi.org/10.1007/s100400050102

GOMO M, DE LANGE F, VERMEULEN D, MOLOKWE TB, BREDEKAMP EG and MOLEME M (2017) Groundwater sampling manual. WRC Report No. TT 733/17. Water Research Commission, Pretoria.

GRAY NF (1996) Field assessment of acid mine drainage contamination in surface and groundwaters. *Environ. Geol.* **27** 358–361. https://doi.org/10.1007/BF00766705

JALALI M (2007) Assessment of the chemical components of Famenin groundwater, western Iran. *J. Environ. Geochem. Health* **29** (5) 357–374. https://doi.org/10.1007/s10653-006-9080-y

JANKOWSKI J and BECK P (2000) Aquifer heterogeneity: hydrogeological and hydrochemical properties of the botany sands aquifer and their impact on contaminant transport. *J. Earth Sci.* **47** (1) 45–64. https://doi.org/10.1046/j.1440-0952.2000.00768.x

KATZ BG, EBERTS SM and KAUFFMAN LJ (2011) Using Cl/Br ratios and other indicators to assess potential impacts on groundwater quality from septic systems: A review and examples from principal aquifers in the United States. *J. Hydrol.* **397** (3–4) 151–166. https://doi.org/10.1016/j.jhydrol.2010.11.017

KATZ BG, GRIFFIN DW and DAVIS JH (2009) Groundwater quality impacts from the land application of treated municipal wastewater in a large karstic spring basin: Chemical and microbiological indicators. *Sci. Total Environ.* **407** (8) 2872–2886. https://doi.org/10.1016/j.scitotenv.2009.01.022

LEA I, WAYGOOD C and DUTHIE A (2003) Water management strategies to reduce long-term liabilities at Grootvlei gold mine. In: *Proceedings of the 8th International Congress on Mine Water & the Environment*, 19–22 October 2003, Johannesburg.

LIGAVHA-MBELENGWA L and GOMO M (2020) Investigation of factors influencing groundwater quality in a typical Karoo aquifer in Beaufort West town of South Africa. *Environ. Earth Sci.* **79** (9) 196. https://doi.org/10.1007/s12665-020-08936-1

LUKAČ REBERSKI J, TERZIC J, MAURICE LD and LAPWORTH DJ (2022) Emerging organic contaminants in karst groundwater: A global level assessment. *J. Hydrol.* **604**. https://doi.org/10.1016/j.jhydrol.2021.127242

MADZIVIRE G, LIGAVHA-MBELENGWA L, NOLAKANA P, VADAPALLI VRK and COETZEE H (2022) Active mine water solutions through relaxing the environmental critical levels of the mine voids in the Witwatersrand Goldfields. Unpublished report. Council for Geoscience, Pretoria.

MAYO AL and LOUCKS MD (1995). Solute and isotopic geochemistry and ground water flow in the central Wasatch Range, Utah. *J. Hydrol.* **172** (1–4) 31–59. https://doi.org/10.1016/0022-1694(95)02748-E

MCCARTHY TS (2006) The Witwatersrand Supergroup. In: Johnson MR, Anhaeusser CR and Thomas RJ (eds.) *The Geology of South Africa*. Geological Society of South Africa, Johannesburg. 691 pp.

MEYBACK M (1987) Global chemical weathering of surficial rocks estimated from river dissolved loads. *Am. J. Sci.* **287** (5) 414–421. https://doi.org/10.2475/ajs.287.5.401

MOKADEM N, DENNIS R and DENNIS I (2021) Hydrochemical and stable isotope data of water in karst aquifers during normal flow in South Africa. *Environ. Earth Sci.* **80** (16). https://doi.org/10.1007/s12665-021-09845-7

PARKHURST DL and APPELO CAJ (1999) User's guide to PHREEQC (version 2) – A computer program for speciation, batch-reaction, one-dimensional transport, and inverse geochemical calculations. Water-Resource Investigations Report 99-4259. United States Geological Survey, Denver.

PAWAR NJ (1993) Geochemistry of carbonate precipitation from the ground waters in basaltic aquifers: an equilibrium thermodynamic approach. *J. Geol. Soc. India* **41** (2) 119–131. https://doi.org/10.17491/jgsi/1993/410202

PIPER A (1944) A graphic procedure in the geochemical interpretation of water-analyses. *Trans. Am. Geophys. Union* **25** (6) 914–928. https://doi.org/10.1029/TR025i006p00914

RAJMOHAN N and ELANGO L (2004) Identification and evolution of hydrogeochemical processes in the groundwater environment in an area of the Palar and Cheyyar River Basins, Southern India. *Environ. Geol.* **46** (1) 47–61. https://doi.org/10.1007/s00254-004-1012-5

SABS (South African Bureau of Standards) (2015) The South African National Standard 241 Drinking Water Specification. SABS, Pretoria.

SCHRADER A (2015) Geohydrological consequences associated with the post-mine closure flooding of dewatered dolomitic karst aquifers in the Far West Rand, South Africa. PhD thesis, North-West University.

SCHRADER A and WINDE F (2015) Unearthing a hidden treasure: 60 years of karst research in the Far West Rand, South Africa. *S. Afr. J. Sci.* **111** (5–6) 1–7. https://doi.org/10.17159/sajs.2015/20140144

SCOTT P, WRENCH B and GELDENHUIS S (1993) Hydrogeological investigations at Enstra. SRK Report 199876/1. SRK, Johannesburg.

SCOTT R (1995). Flooding of Central and East Rand Gold mines: An investigation into control over the inflow rate, water quality and the predicted impacts of flooded mines. WRC Report No. 486/1/95. Water Research Commission, Pretoria.

TUCKER RF, VILJOEN RP and VILJOEN MJ (2016) A review of the Witwatersrand Basin – the world's greatest goldfield. *Episodes* **39** (2) 105–133. https://doi.org/10.18814/epiiugs/2016/v39i2/95771

VENGOSH A and KEREN R (1996) Chemical modifications of groundwater contaminated by recharge of treated sewage effluent. *J. Contam. Hydrol.* **23** (4) 347–360. https://doi.org/10.1016/0169-7722(96)00019-8

WILCOX LV (1955) Classification and use of irrigation waters. United States Department of Agriculture, Washington DC.

WHO (World Health Organization) (2022) Guidelines for Drinking-Water Quality: Fourth Edition Incorporating the First and Second Addenda. WHO, Geneva.